Society For Biomaterials

Degradation and biocompatibility of multistage nanovectors in physiological systems

Jonathan O. Martinez,[1,2] Michael Evangelopoulos,[1] Ciro Chiappini,[1,3]* Xuewu Liu,[1] Mauro Ferrari,[1] Ennio Tasciotti[1]

[1]Department of Nanomedicine, Houston Methodist Research Institute, 6670 Bertner Ave., Houston, Texas 77030
[2]Graduate School of Biomedical Sciences, University of Texas Health Science Center, 6767 Bertner Ave., Houston, Texas 77030
[3]Department of Biomedical Engineering, University of Texas at Austin, 107 W. Dean Keeton, Austin, Texas 78712

Received 1 July 2013; revised 16 September 2013; accepted 22 October 2013
Published online 16 November 2013 in Wiley Online Library (wileyonlinelibrary.com). DOI: 10.1002/jbm.a.35017

Abstract: The careful scrutiny of drug delivery systems is essential to evaluate and justify their potential for the clinic. Among the various studies necessary for preclinical testing, the impact of degradation is commonly overlooked. In this article, we investigate the effect of fabrication (porosity and nucleation layer) and environment (buffer and pH) factors on the degradation kinetics of multistage nanovectors (MSV) composed of porous silicon. The degradation by-products of MSV were exposed to endothelial cells and analyzed for detrimental effects on cellular internalization, architecture, proliferation, and cell cycle. Increases in porosity resulted in accelerated degradation exhibiting smaller-sized particles at comparable times. Removal of the nucleation layer (thin layer of small pores formed during the initial steps of etching) triggered a premature collapse of the entire central porous region of MSV. Variations in buffers prompted a faster degradation rate yielding smaller MSV within faster time frames, whereas increases in pH stimulated erosion of MSV and thus faster degradation. In addition, exposure to these degradation by-products provoked negligible impact on the proliferation and cell cycle phases on primary endothelial cells. In this study, we propose methods that lay the foundation for future investigations toward understanding the impact of the degradation of drug delivery platforms. © 2013 Wiley Periodicals, Inc. J Biomed Mater Res Part A: 102A: 3540–3549, 2014.

Key Words: degradation, porous silicon, multistage nanovectors, drug delivery, cytocompatibility

How to cite this article: Martinez JO, Evangelopoulos M, Chiappini C, Liu X, Ferrari M, Tasciotti E. 2014. Degradation and biocompatibility of multistage nanovectors in physiological systems. J Biomed Mater Res Part A 2014:102A:3540–3549.

INTRODUCTION

In the past decade, porous silicon (pSi) has gained significant momentum within the biomedical field because of desirable traits such as favorable degradability,[1] biocompatibility,[2] and photoluminescence.[3] These unique set of qualities allowed pSi to be applied to applications ranging from optics[4] and biosensors[5] to microelectronics[6] and tissue engineering.[7,8] Moreover, the flexible nature of pSi permits the adjustment of fabrication parameters to modify precise characteristics (e.g., size, shape, surface, pore size) and has made pSi particularly favorable for drug delivery applications. For example, by leveraging the increased surface area and pore volume of pSi vectors, the secure attachment and incorporation of various molecules, therapeutic moieties, and nanoparticles was successfully achieved.[9–11] This inherent versatility allowed pSi vectors to increase the bioavailability and drug solubility and provide prolonged release of various payloads.[12]

pSi has the unique ability to degrade completely yielding a bioinert[13] silicic acid as its only product. As demonstrated in previous studies, silicic acid is fundamental for normal bone homeostasis, and increased levels of silicic acid were well sustained within the body and readily excreted through urine.[14] In addition, advantageous health benefits have been witnessed in silicic acid's rare ability to reduce aluminum uptake and promote increased excretion of aluminum in urine,[15] which can be beneficial for the prevention and progression of Alzheimer's disease.[16] Previous studies have also demonstrated silicic acid's ability to stimulate the synthesis of collagen type 1 and promote osteoblastic differentiation.[17] These many advantages provided by pSi

Additional Supporting Information may be found in the online version of this article.
*Present address: Department of Materials, Imperial College London, Prince Consort Rd, London, SW7 2AZ, UK
Correspondence to: E. Tasciotti; e-mail: etasciotti@tmhs.org
Contract grant sponsor: The Defense Advanced Research Projects Agency (DARPA); contract grant number: W911NF-11-1-0266
Contract grant sponsor: The Alliance for NanoHealth, specifically DOD TATRC; contract grant numbers: W81XWH-09-2-0139 and W81XWH-10-2-0125
Contract grant sponsor: TMHRI and the Ernest Cockrell Jr. Distinguished Endowed Chair
Contract grant sponsor: NIH; contract grant number: 5F31CA154119-02 (to J.O.M.)

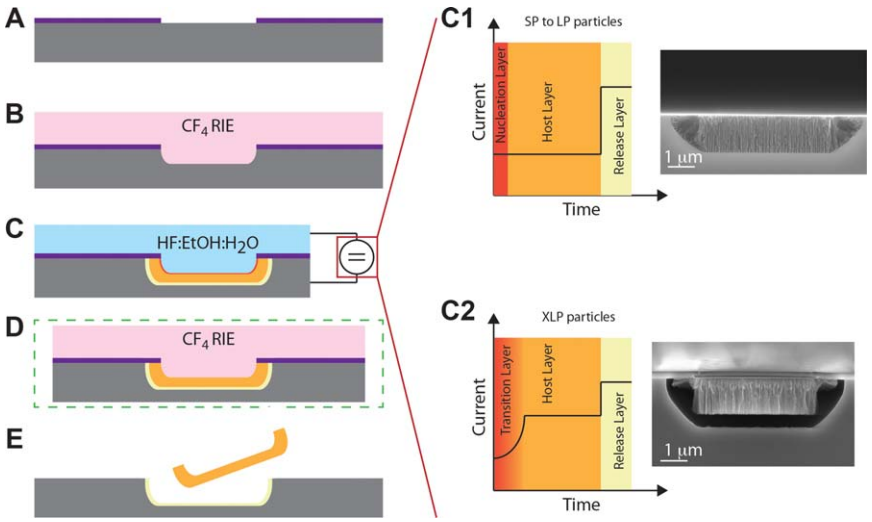

FIGURE 1. Schematic representation of the MSV fabrication process. (A) Fabrication began with a silicon rich silicon nitride layer. (B) Patterning in CF_4 yielded an array of 2 μm diameter holes with pitch of 2 μm. (C) A reactive ion etch formed pores corresponding to photolithographic holes from the previous step. Graphs on right show the effect of current applied over time for SP to LP (top) and XLP (bottom) with SEM images depicting porosity. (D) The optional removal of the nucleation layer was performed in a reactive ion etch with CF_4. (E) MSV particles were released after etch with CF_4. [Color figure can be viewed in the online issue, which is available at wileyonlinelibrary.com.]

by-products allow pSi to be a suitable material for drug delivery applications.

Thus, by taking advantage of the numerous features of pSi, our group successfully engineered[18] and tested[19–21] multistage nanovectors (MSV) whose primary objective was to decouple the multiplicity of tasks required for the delivery of therapeutics to specific locations and distribute them onto separate stages. Within this platform, pSi performs as the first stage and is tasked to carry, protect, deliver, and release the second stage in an efficient manner. The adjustment of fabrication parameters enables the creation of pore sizes ranging from 3 to 100 nm in diameter to accommodate the loading of various sized payloads.[18] In addition, to ensure increased retention within the pores, a nucleation layer is incorporated to prevent payloads from passing freely through the pores. Although both properties serve to enable the greatest efficacy of a payload-loaded MSV, the characteristics that regulate their degradation have yet to be fully investigated.

In addition to efficiency and safety, a major consideration for drug delivery systems is their ability to be compatible within the body's environmental conditions and maintain stability for systemic administration. Although previous work examined the degradation effect of pegylation[22] and biofluids[23] on pSi, this work aims to investigate the degradation dynamics of MSV to understand their stability at different porosities, removal of the nucleation layer, and impact of buffer and pH. Furthermore, the consequences of MSV degradation by-products on cellular architecture, proliferation, and cell cycle were explored. Herein, we monitored the impact of fabrication (porosity, nucleation layer) and environmental (buffer, pH) parameters on the degradation of MSV using inductively coupled plasma – atomic emission spectrometer (ICP-AES), scanning electron microscopy (SEM), flow cytometry, and size and zeta potential analysis. In addition, the cytocompatibility of MSV was assessed using primary cells to assess detrimental effects on cell structure, proliferation, and cell cycle.

MATERIALS AND METHODS

MSV fabrication

We previously reported how combining microfabrication with electrochemical etching yielded the MSV[18] used in this study (Fig. 1). An initial deposition of a 120-nm thick layer of silicon-rich silicon nitride (SiN) over a 100-mm p-type Si wafer [Fig. 1(A)] followed by photolithography yielded an array of 2 μm diameter holes with 2 μm pitch [Fig. 1(B)]. Reactive ion etching (RIE) in CF_4 gas formed 400 nm deep trenches in the Si corresponding to the photolithographic holes [Fig. 1(C)]. Stripping of photoresist followed by electrochemical etching with the SiN masking layer formed MSV in the 2 μm × 400 nm trenches [Fig. 1(D)]. The current profile during electrochemical etching and the composition of the etch solution determined the porosity and shell thickness of the MSV. A two-step current process yielded MSV with small to large pores [SP-LP; Fig. 1(C)]. The initial step used a lower current to form the nucleation layer and following host layer. The nucleation layer was a $<$50 nm thick layer of pores $<$2 nm in diameter that inevitably forms in the initial steps of electrochemical etch. A step up in current formed an unstable pSi layer with high porosity between the host layer and the solid silicon substrate. Once the electrochemical process was completed, the substrates were washed and dried in N_2. At this step, it was possible to remove the nucleation layer, if desired, through a short RIE in CF_4 gas [Fig. 1(E)]. Release of MSV from the substrate was achieved by shattering the release layer through sonication in isopropanol [Fig. 1(F)]. Extra large pore (XLP) MSV consisting exclusively of a host layer were not mechanically stable because of the $>$80% porosity of the layer. For this reason, the

formation of MSV with XL pores instead required the initial formation of a transitional layer with ~80 nm thickness having pores of progressively increasing diameter, which varied from that of the nucleation layer to that of the XLP host layer [Fig. 1(C)]. To achieve this, an initial step with progressively increasing current was introduced before the two-step current process. These studies were conducted using 3.2 × 0.7 μm MSV with various porosities dependent on study.

Degradation of MSV

MSV with varying porosities and presence of a nucleation layer was studied by inducing degradation in phosphate-buffered saline (PBS) under rotation using a LabQuake tube rotator at 10 rpm and 37°C, pH 7.2.[24] At predetermined times, aliquots were removed from samples, centrifuged at 4200 rpm for 10 min, and supernatants were discarded. Aliquots were stored at 4°C until analysis could be performed. NP, SP, MP, LP, and XLP were used to study the effect of porosity, and MP was selected to study the contribution of a nucleation layer. Effect due to buffers was investigated comparing Tris-HCl 20 m*M* pH 7.3 + 0.9% NaCl (Sigma-Aldrich) as the "saline" solution and Dulbecco's modified eagle medium (GIBCO) supplemented with 10% fetal bovine serum (GIBCO) as the "cell culture media" (CCM) solution. To investigate the effect of buffer, SP and LP MSV were selected to have a range of MSV porosities tested. A total of 1.2×10^7 MSV (SP & LP) was suspended in 1.5 mL of saline or CCM solution and measured in triplicate. Degradation was studied as previously mentioned with samples under rotation at 10 rpm at 37°C. One rotational speed was chosen to concentrate on the differences between fabrication and environmental factors rather than the effect rotation may have. The effect attributed to pH was investigated by adjusting 20 m*M* Tris-HCl to various pH levels. A total of 1.5×10^6 LP MSV were suspended in 1.5 mL of each pH and rotated at 37°C.

For flow cytometry, aliquots were resuspended in deionized water and measured using a BD FACSCalibur (BD Biosciences) and analyzed with CellQuest. For ICP-AES, aliquots were placed in nylon centrifugal filter tubes (0.45 μm, VWR) and centrifuged for 10 min at 4200 rpm. Samples were diluted 1:100 in water containing 1 ppm of Yttrium and measured on a Varian Vista Pro Simultaneous Axial at the Geochemistry Laboratory at Rice University. MSV size distribution and number were examined using the Z2™ COULTER COUNTER® Cell and Particle Counter outfitted with a 50-μm ampoule aperture tube (Beckman Coulter; Fullerton, CA). Samples were diluted into 1.0 mL of ISOTON and counted using limits of 1.0 to 2.8 μm, with the resulting data exported to Excel. Samples for SEM were washed twice in water to remove salts from samples and resuspended in 25 μL of water and placed in the center of an aluminum stage. Samples were left to dry overnight in a vacuum desiccator. Images were taken on a Zeiss Neon 40 microscope equipped with an in-lens detector. Zeta potential measurements were resuspended in 1.5 mL of filtered monobasic PB (10 m*M*, pH 7.4) and measured using a ZetaPALS analyzer (Brookhaven Instruments Corporation; Holtsville, NY).

Cell culture

Human umbilical vein endothelial cells (HUVEC) were purchased from Lonza (Lonza Group, Switzerland) and cultured in Clonetics® EBM®−2 Endothelial Cell Growth Medium-2 (Lonza; CC-3156) supplemented with EGM-2 SingleQuots® Kit (Lonza; CC-4176). HUVEC were used between passages 4 and 10 for described experiments.

MTT and cell cycle

For MTT, HUVEC were seeded in 96 well plates at 5000 cells per plate. Degradation by-products collected from the supernatant of completely degraded MSV were added to each well. At predetermined times, wells were incubated with 3-[4,5-Dimethylthiazol-2-yl]-2,5-Diphenyltetrazolium Bromide (MTT) at 0.5 mg/mL in complete media for 2 h at 37°C, 5% CO_2 followed by an 30 min incubation with dimethyl sulfoxide and measured for absorbance at 570 nm on a BioTek plate reader.

The effect on cell cycle after treatment with the by-products of degradation from MSV was evaluated as previously described.[25] In brief, HUVEC were treated with SP or LP MSV degraded by-products by completely degrading MSV and removing samples from the degraded supernatant portion (i.e., not partially degraded MSV). At predetermined times, cells were collected and quickly fixed using 70% ethanol at 4°C for 10 min and then stored at −20°C for 30 min. A 50 μg/mL solution of propidium iodide (PI) was prepared in a 10 m*M* Tris buffer at pH 7.3 containing 5 m*M* $MgCl_2$. 1 mL of PI solution and 50 μL of a 1.5-mg/mL solution of RNAse I were slowly added under gentle agitation. Cells were incubated for 1 h at 37°C, followed by three washes in PBS, resuspended in 200 μL, and analyzed using a Becton Dickinson FACSCalibur.

HUVEC cytoskeletal staining

HUVEC were seeded into a chamber slide (LabTek) at 75,000 cells per well and allowed to adhere overnight. The following day, HUVEC were treated with DyLight® 555 MSV at a ratio of 1:10 and an equivalent amount of MSV fragments (i.e., partially degraded MSV) for 24 h. HUVEC were then stained with AlexaFluor 488 Phalloidin (Invitrogen), mounted with Pro Long Gold containing DAPI, and imaged using an inverted Nikon Eclipse Ti microscope.

Statistical analysis

All statistics were calculated using Prism GraphPad software. Zeta potential values were tested using a two-way analysis of variance followed by a Bonferroni post-test to compare NP to SP and MP. Nonlinear regression analysis fitted with a one-phase association equation using the least squares method was used to test significance in ICP-AES data [Fig. 3(D) and Fig. 4(A)]. Constraints of Y_0 at 0.0 and plateau equal to 100 were used, and the resulting rate constants were compared using an extra sum of squares F test. For MTT results (Fig. 6), linear regression analysis was performed and significance was determined by testing whether the slopes and intercepts were significantly different (F test). In all cases: * was used for p values between

TABLE I. MSV Characteristics

Name of MSV	Porosity (%)	Pore Size (nm)
Nonporous (NP)	0	0
Small pore (SP)	46	10.1
Medium pore (MP)	51	15.2
Large pore (LP)	66	26.3
Extra large pore (XLP)	82	51.3

0.01 to 0.05, ** for values between 0.001 to 0.01, and *** for values <0.001.

RESULTS AND DISCUSSION

Impact of porosity on MSV degradation

The flexible nature of MSV allows for tunable porosity to accommodate a variety of payloads and thus can have critical implications for drug delivery. This impact was studied by comparing five different conditions (Table I): NP (nonporous), SP (small pores), MP (medium pores), LP (large pores), and XLP (extra large pores). Differences in degradation profiles were investigated using size and zeta potential analysis at several times. Figure 2(A) compared the volume distributions of various MSV at different time points. The distributions were offset on the y-axis for clarity and to compare the changes in size at different times. The initial peak at 1 fL was the detection limit of the instrument and was common to all MSV examined. As MSV degraded, a shift in their volume toward the detection peak is apparent for all MSV with the exception of NP. These shifts appeared earlier for MSV with higher porosities and whose peaks progressed closer to the detection limit at a faster rate. Figure 2(B) substantiates this claim by normalizing to zero hours and plotting the modes (e.g., highest occurring number) collected during volume analysis. As time increased, we observed the same trend as the volume graphs where the more porous MSV displayed an overall smaller size at each time point, whereas NP experienced minimal changes in size. For example, at 24 h, the size of MSV had decreased by 37, 56, 62, and 70%, respectively, for SP, MP, LP, and XLP.

Zeta potential measurements were performed to determine the surface charge of MSV as they degraded. Figure 2(C) shows the changes in surface charge of NP, SP, and MP MSV during degradation. Because of their (3-aminopropyl)-triethoxysilane (APTES) modification, MSV were initially imparted with a positive charge (+10–15 mV) and with time MSV became highly negative (−25 to 30 mV). At 8 h, MSV reached a plateau of negative charge of −40 mV and −35 mV for NP and SP/MP, respectively. By 24 h, the

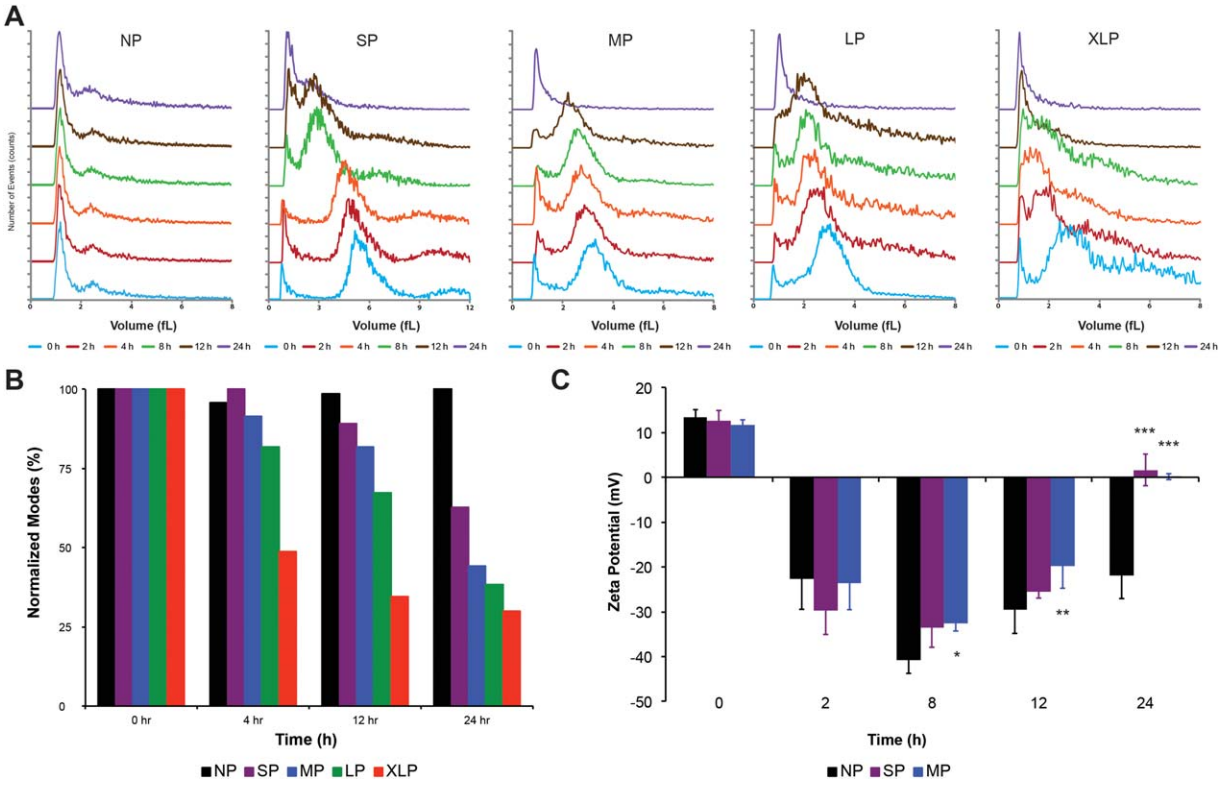

FIGURE 2. Effect of porosity on degradation of MSV. (A) Volume distributions of MSV with varying porosities are plotted at various times comparing the shifts in size. Distributions are offset on the y-axis to highlight differences between time points. (B) The mode, or the value that appears most frequent, at each time point is plotted and compared with other porosities of MSV. NP serves as control, as degradation of nonporous silicon particles is minimal and was used for comparison. (C) Zeta potential measurements were used to provide insight on the surface charge of NP, SP, and MP MSV. The results are shown as mean ± SD. Asterisks denote data points where the difference was statistically significant compared with NP. *$p<0.05$, **$p<0.01$, ***$p<0.001$. [Color figure can be viewed in the online issue, which is available at wileyonlinelibrary.com.]

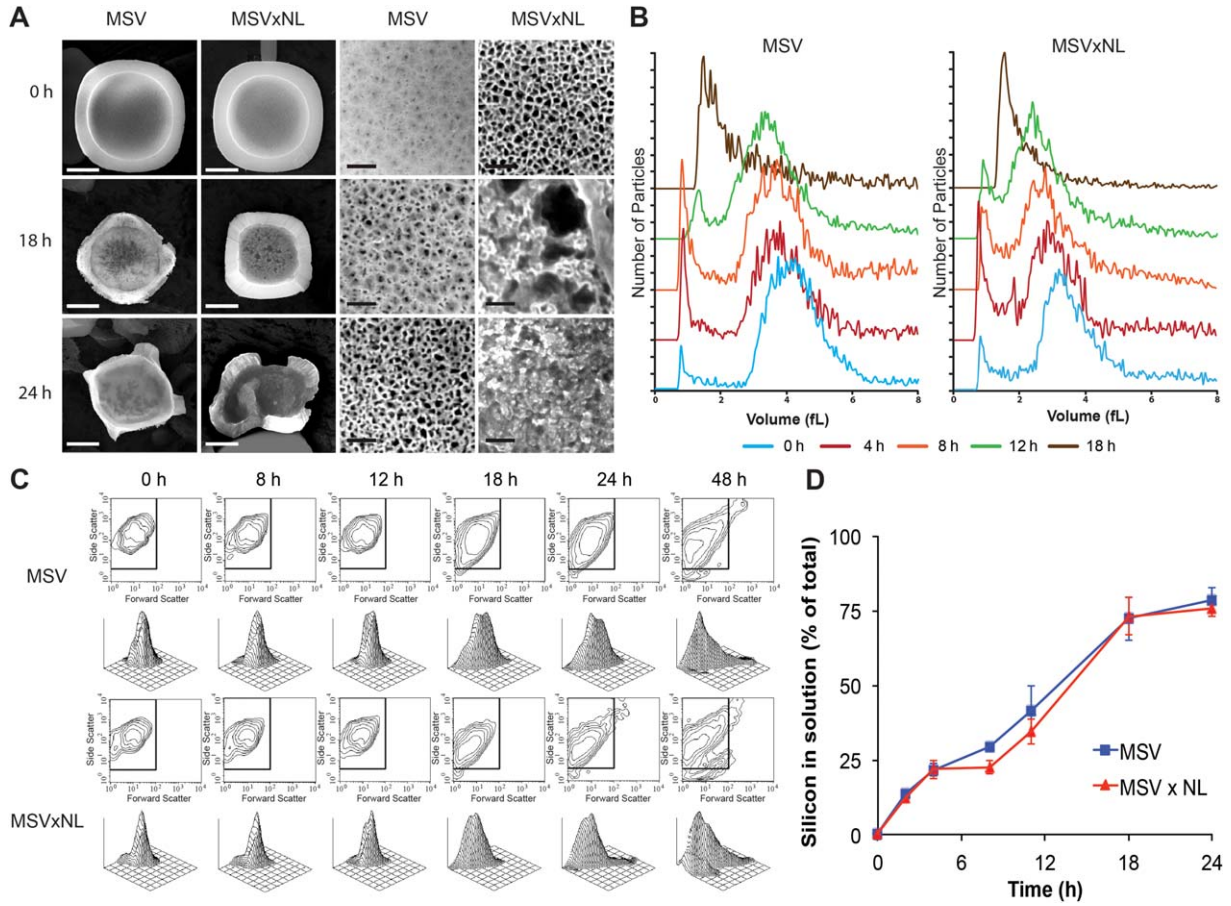

FIGURE 3. The impact of the nucleation layer on pore stability. (A) MSV with and without a nucleation layer (MSVxNL) were compared at various times looking at the overall effect on size and shape (left) and their pores (right) on the front-side where the nucleation layer is visible. Scale bars, left for particle is 1 μm; right for pores is 50 nm. (B) Volume distribution of MSV and MSVxNL showing smaller sized for MSVxNL but with comparable shifts in size with increased time. (C) Flow cytometry verifying similar patterns for size (forward scatter) and shape (side scatter) of the two MSV. (D) ICP-AES contrasting MSV versus MSVxNL to confirm minimal change in overall degradation of MSV without nucleation layer. [Color figure can be viewed in the online issue, which is available at wileyonlinelibrary.com.]

surface charges of SP and MP were neutral, whereas NP remained negative (significantly different from SP and MP). Hence, as the porosity of MSV increased, an equivalent increase in degradation rate was observed. Surface charge measurements revealed that the APTES surface modification quickly degraded and exhibited a pattern such that the highest value was achieved at 8 h potentially indicating the point where the highest surface area existed. On the other hand, the surface charge measurements of NP MSV remained consistent confirming minimal degradation over time.

Absence of nucleation layer and effect on pore structure

A critical function for MSV is to load and retain a nanoparticle payload within its porous structure. The nucleation layer serves to prevent payloads from passing freely through MSV and is typically associated with pore sizes less than 2 nm. We investigated the impact on MSV degradation by comparing SEM, ICP-AES, flow cytometry, and size analysis. SEM images illustrated that MSV without a nucleation layer (MSVxNL) began with larger pores on the front-side while retaining the same overall shape compared with regular MSV [Fig. 3(A)]. The overall shape of MSV and MSVxNL remained similar over time. However, we observed that the porous structure of MSVxNL displayed significant remodeling such that by 18 h considerably larger pores were observed. This resulted in premature pore instability ultimately triggering their complete collapse by 24 h [Fig. 3(A)]. As shown in Figure 3(B), the size distribution of MSVxNL began with slightly smaller sizes consistent with the earlier results of higher porosity MSV. The shifts in size over time associated with MSVxNL were comparable to the variations observed in conventional MSV containing a nucleation layer. Flow cytometry [Fig. 3(C)] confirmed that MSVxNL size (forward scatter, FSC) and shape (side scatter, SSC) degraded in a manner consistent with classical MSV. FSC and SSC contour and 3D plots illustrated similar patterns with analogous shifts accumulating at the origin of the graphs, indicative of MSV degradation between 24 and 48 h. In addition, ICP-AES [Fig. 3(D)] confirmed that MSVxNL had minimal effect on the overall degradation of MSV as no significant increase in Si was detected in solution determined using nonlinear regression analysis and comparing rate constants. The absence of a

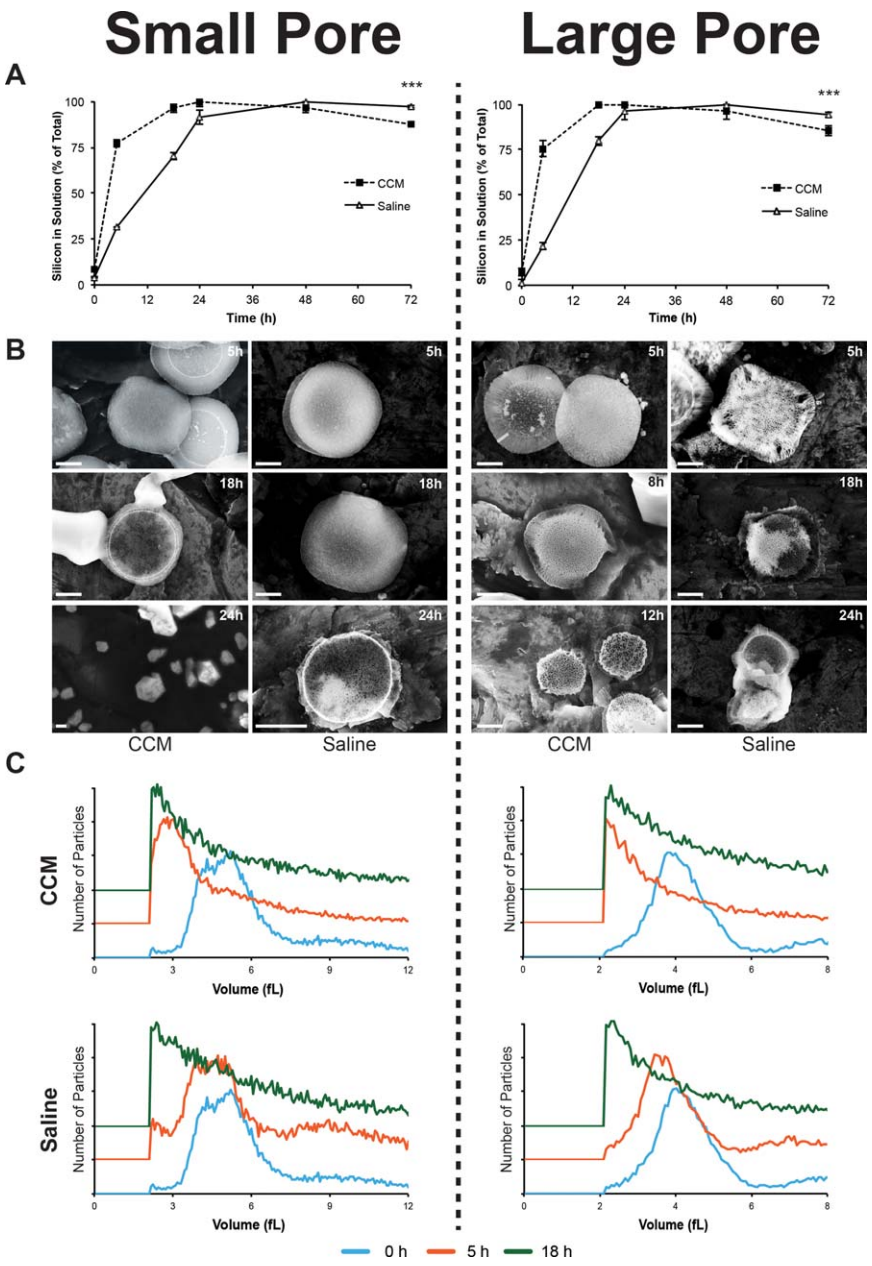

FIGURE 4. Influence of buffer in degradation of MSV. (A) ICP-AES comparison of MSV, SP (left column) and LP (right column), degradation in CCM and saline solution. (B) SEM images showing MSV degradation in CCM (left) and saline (right) solutions at various time points. (C) Volume distributions of MSV in CCM (top) and saline (bottom) are plotted at various time points relating the shifts in size. Distributions are offset on the y-axis to highlight differences between time points. The results are shown as mean ± SD. Asterisks denote where the difference was statistically significant compared with saline. ***$p < 0.001$. [Color figure can be viewed in the online issue, which is available at wileyonlinelibrary.com.]

nucleation layer from MSV had a negligible effect on their overall degradation pattern resulting in comparable changes in size and shape. However, the porous structure of MSV experienced a remarkable difference in their degradation displaying increased instability generating increased porosity in the core of MSV resulting in complete pore collapse by 24 h. Although the absence of a nucleation layer may negatively impact payload loading or retention, it may be beneficial to achieve a quicker release rate attributed to the quicker pore breakdown observed.

Degradation behavior of MSV in varying buffers

An understanding of the interplay between the local environment and the effect on the degradation of drug delivery vectors is vital to gauge its use for systemic administration. To this extent, we compared the degradation kinetics of MSV in two different types of buffers: DMEM with 10% fetal bovine serum (FBS) (CCM) and Tris-HCl + 0.9% NaCl (Saline), both at pH 7.3. SP and LP MSV were investigated to discover the impact of buffer on degradation using ICP-AES, SEM, and size analysis. Figure 4(A) demonstrated that

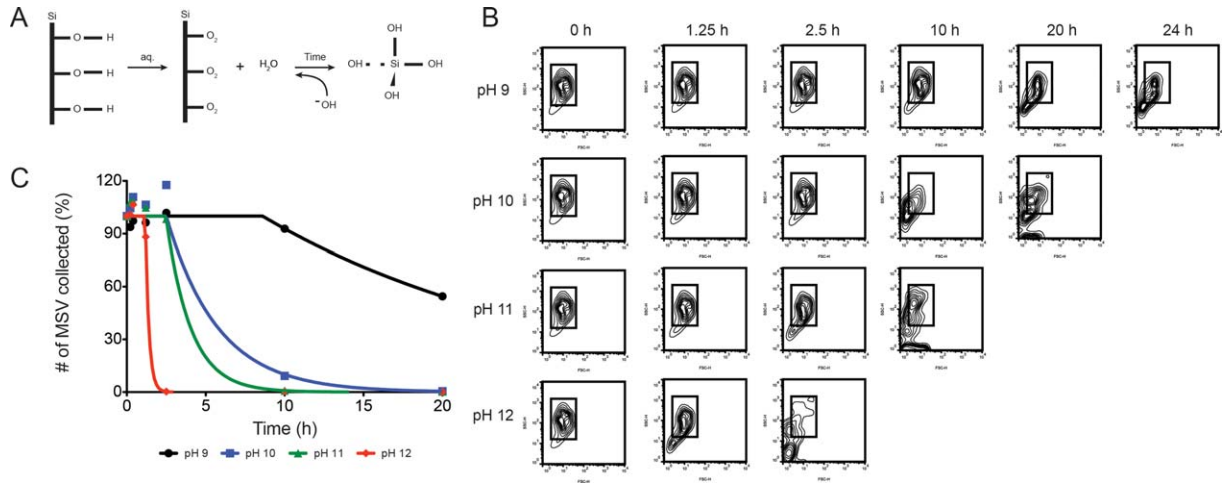

FIGURE 5. Degradation effect of MSV in varying pH environments. (A) Schematic showing possible interactions between the MSV surface and hydroxyl groups. Hydroxyl ions of an alkaline solution weaken the surface of the MSV forming bioinert silicic acid. (B) Flow cytometry exhibiting distinct patterns and changes in size (forward scatter) and shape (side scatter) exposed to the varying pH environments. (C) Flow cytometer counts collected at various time points to show degradation rates of MSV at pHs between 9 and 12. [Color figure can be viewed in the online issue, which is available at wileyonlinelibrary.com.]

when suspended in CCM, the overall degradation process was accelerated for both SP and LP. In CCM, SP reached a plateau of maximum Si deposition by 24 h, whereas in saline, this was not achieved till 48 h (90% at 24 h). Similarly, LP reached plateaus at 18 h in CCM and 48 h in saline (80% at 24 h). Nonlinear regression analysis revealed that MSV in CCM experienced a significant acceleration in degradation rate, such that they degraded more than 3.5× faster in CCM compared with saline for both SP and LP. Furthermore, SEM images [Fig. 4(B)] confirmed that both SP and LP degraded quicker in CCM compared with saline. In CCM, MSV exhibited marked transformations in the overall appearance displaying smaller sized particles at 18 and 24 h for SP and 12 versus 24 h for LP. Figure 4(C) validated that marked shifts in size were observed for MSV in different buffers. Both SP and LP in CCM experienced a substantial shift within 5 h resulting in acquisition of MSV predominantly at the lower detection limit, which was not the case for MSV in saline. Thus, MSV exposed to CCM revealed accelerated degradation kinetics resulting in substantial structural instability and shifts in size compared with MSV in saline buffers. The addition of amino acids and serum proteins commonly found in CCM[26] and FBS possibly contributed to increased degradation. The disparity between CCM and saline suggests that MSV will experience a significant increase in degradation upon encountering sites rich in proteins, amino acids, and salts such as the tissue and cellular microenvironment and during systemic blood circulation.

pH-induced degradation of MSV

Comprehension of the degradation phenomenon governing MSV in varying pH environments is essential to ensure stability during systemic administration and upon interactions within cellular environments. The influence of pH on MSV degradation was investigated using a range from 9 to 12. In alkaline solutions, the adsorption of hydroxyl ions on Si produces its dissolution into orthosilicic acid as the concentration of hydroxyl ions are increased.[27] This favors the formation of a bioinert neutral monomer of silicate ions as equilibrium is reached that plays a beneficial role in the optimal growth of bone and collagen.[28] MSV degradation in alkaline conditions can be represented as shown in Figure 5(A). In an aqueous solution, the hydroxyl layer of the MSV undergoes weak nucleophilic attack by the water molecules. Increasing the pH of the solution, therefore, provides a stronger nucleophilic attack that ultimately produces accelerated degradation of MSV into silicic acid. As shown in Figure 5(B), the contour plots acquired by flow cytometry displayed progressive loss of organization of the overall shape and size of MSV as pH increased, indicated by the increase of particles located outside the gating box. The ROI box within the plots was used to monitor the extent of degradation, such that as MSV degrade their distribution will extend outside of the box and drift toward the origin where small fragments accumulate. MSV experienced substantial effects on the size and shape in 24 h dependent on the pH used. At pH 12, MSV began drifting at 2.5 h while at pH 10 manifestations were not apparent until 20 h. Next, we compared the total counts collected by the flow cytometer at various times [Fig. 5(C)]. This was performed by fitting the data using a plateau followed by a one-phase exponential decay constraining the plateau to 0 and Y_0 to 100, complete parameters detailed in supplementary information. At increasing pH, MSV revealed an accelerated degradation with fewer MSV collected at increasing pH levels. We fitted the data using a plateau followed by a one-phase exponential decay constraining the plateau to 0 and Y_0 to 100. This resulted in distinct degradation rate constants of 0.053, 0.306, 0.638, and 4.45 h^{-1} for pH 9, 10, 11, and 12, respectively. In addition, this model calculated delays in the initiation of degradation (X0) such that as the pH increased the

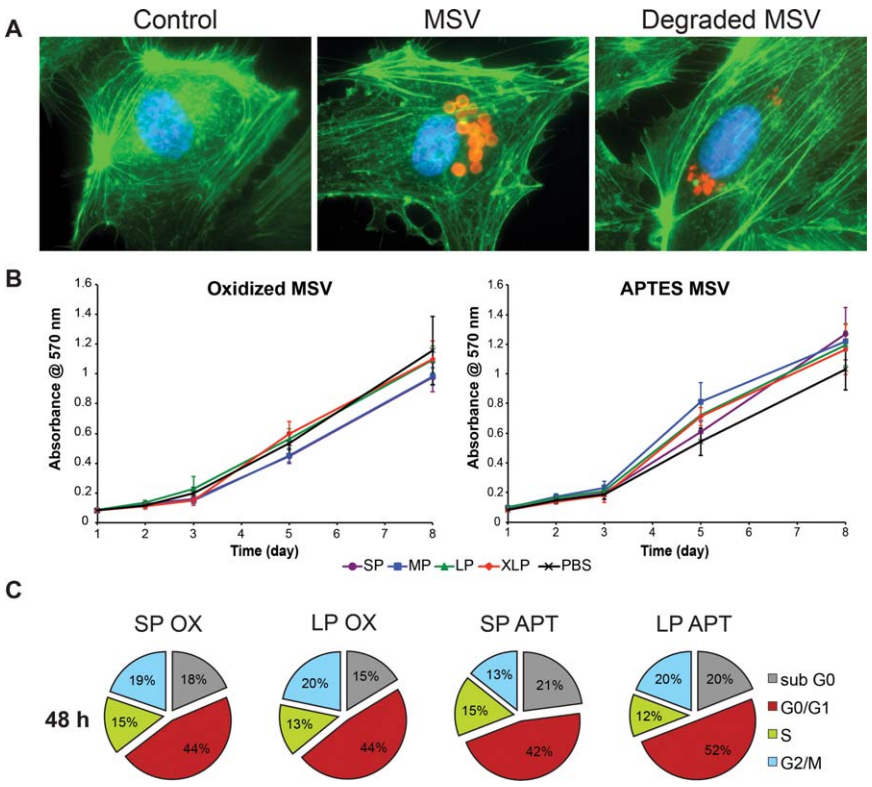

FIGURE 6. Cellular architecture and biocompatibility of MSV degradation products. (A) The microfilaments (green) and nucleus (blue) of HUVEC were stained to interpret the effect of exposing MSV fragments. Control and nondegraded MSV were used to compare cytoskeletal structure. (B) An MTT assay to demonstrate the continued proliferation of HUVEC after internalizing oxidized (left) and APTES (right) degradation products of MSV with varying porosities (SP-XLP). Proliferation of HUVEC was compared with sterile PBS, the buffer used to degrade the MSV. The results are shown as mean ± SD. (C) Cell cycle analysis at 48 h after introduction to degradation products of MSV. The cell cycle of HUVEC was conserved independent of surface (oxidized and APTES) and porosity (SP and LP). [Color figure can be viewed in the online issue, which is available at wileyonlinelibrary.com.]

decay began earlier with times ranging from 1.2 to 8.6 h. Taken together, this data demonstrated that the increasing concentrations of hydroxide ions resulted in a rapid degradation on the surface of MSV producing considerable structural modifications. As the solution became more basic, the strength of the nucleophilic attack intensified resulting in an overall increase in exposed pSi surface area and ultimately yielding the final product of orthosilicic acid.

Cellular uptake and architecture

The concerns regarding the exposure of nanovectors to healthy cells must be adequately examined to gauge its potential use in the clinic. We investigated the reaction of HUVEC cultures upon introduction to partially degraded MSV (i.e. fragments). We initially sought to understand the impact the internalization of fragments have on the cell architecture, specifically inspecting the microfilaments of the cytoskeleton. Hence, we compared the f-actin staining of HUVEC treated with equal concentrations of intact MSV and MSV fragments. As shown in Figure 6(A), the microtubules (green) and nucleus (blue) of HUVEC displayed similar staining, comparing untreated and MSV. HUVEC exhibited conserved parallel filamentous microfilament arrangements that assembled equally throughout the entire cell. Previous studies demonstrated that MSV were quickly delivered to the perinuclear region.[25] Similarly, MSV fragments were found to preferentially accumulate around the perinuclear area. Furthermore, nuclear staining revealed consistent shapes upon internalization indicating a negligible cytotoxic effect attributed to fragments. Thus, internalization of MSV degradation by-products exhibited a negligible effect on cellular architecture producing conventional endothelial phenotypes.

Maintained cellular integrity

Understanding the potential consequences of complete degradation by-products on normal cellular homeostasis is crucial for evaluating drug delivery vectors. The impact of degradation products on the proliferation and cell cycle maintenance of HUVEC was investigated by exposing cells to completely degraded MSV. The proliferation of HUVEC was studied by comparing the incorporation of MTT to extrapolate the level of metabolic activity. Degraded products from oxidized and APTES MSV exhibited similar proliferation rates when compared with PBS controls [Fig. 6(B)]. HUVEC displayed a resilient response to the degradation by-products of MSV of varying porosities (SP, MP, LP, XLP) preserving an active mitochondrial function. In addition, linear

regression analysis revealed that the proliferation rates (i.e., slopes) of HUVEC exposed to oxidized and APTES modified MSV were not significantly different than the PBS control. The different porosities demonstrated that HUVEC tolerated a wide concentration of Si approximately ranging from 30 to 80 pg/cell for XLP to SP, respectively.

Although comprehending the metabolic activity and continued proliferation of cells is useful, it fails to provide detailed information on specific events occurring within cells upon exposure. As shown in Figure 6(C), we quantified the percentage of HUVEC within the different phases of the cell cycle at 48 h comparing the effect of degradation products with different surface chemistry and porosities. HUVEC revealed equivalent patterns of distribution across the phases at 48 h with similar quantities among the different groups. A comparison of these results with control and intact MSV[25] revealed that at 48 h HUVEC exposed to the degradation products of MSV behaved nearly identical. Control HUVEC displayed 17% in the sub G_0 phase, commonly where apoptotic/inactive cells are categorized, comparable with cells containing MSV degradation products whose values ranged from 15 to 21%. Furthermore an inspection of combined effort of the G_2/M and S phases of the cycle, representative of mitotic and DNA replication, respectively, can be used to chronicle the 'active' fraction of cell division. Using this benchmark, we confirmed that HUVEC preserved these routine functions in a consistent manner displaying 32% for control cells and ranging from 28 to 34% for MSV degradation. In addition, analogous HUVEC percentages were discovered in the G_0/G_1 phase, which recognizes cells in the resting/checkpoint stage. Hence, exposure to MSV degradation products yielded a negligible cellular response from primary endothelial cells. In fact, we recently demonstrated that intact MSV would permit HUVEC and stem cells to conserve their intrinsic functions (e.g., tube formation and multipotent differentiation) upon internalization confirming a higher degree of biocompatibility.[29] Here, HUVEC maintained proliferation and routine cycling through various cellular phases without influencing DNA replication for several days after the introduction of the degradation products.

CONCLUSION

In summary, we have reported how MSV were influenced by both fabrication and environmental elements and how the degradation products affected normal cellular viability and integrity. This study can potentially serve as a model on how to characterize drug delivery vectors to achieve optimal degradation profiles while maintaining minimal impact on biological systems. Variations in MSV porosity resulted in substantial shifts in size and shape producing faster degrading MSV as the porosity increased. The removal of the nucleation layer significantly impacted the stability of pore structure generating an early collapse of the pores. Environmental influences also dictated how MSV would behave such that buffers containing amino acids and proteins (e.g., CCM) and an increase in pH facilitated quicker degradation of MSV. The degradation by-products of MSV were well tolerated and exhibited minimal effect on the cellular architecture, proliferation, and cell cycle progression of HUVEC. The work presented here establishes a precedent for future studies to investigate the impact the degradation of drug delivery vectors has on biological systems.

ACKNOWLEDGMENTS

The authors would like to thank Glen Snyder (Rice University) for sample measurement by ICP-AES, David Haviland (TMHRI) for flow cytometry assistance, Matthew Landry (TMHRI) for excellent graphical support, and Kevin Plant for technical assistance.

REFERENCES

1. Canham LT. Bioactive silicon structure fabrication through nanoetching techniques. Adv Mater 1995;7:1033–1037.
2. Bayliss SC, Heald R, Fletcher DI, Buckberry LD. The culture of mammalian cells on nanostructured silicon. Adv Mater 1999;11: 318–321.
3. Pavesi L, Ceschini M, Rossi F. Photoluminescence of porous silicon. J Lumin 1993;57:131–135.
4. Pavlikov AV, Lartsev AV, Gayduchenko IA, Yu Timoshenko V. Optical properties of materials based on oxidized porous silicon and their applications for UV protection. Microelectron Eng 2012; 90:96–98.
5. Ko PJ, Ishikawa R, Takamura T, Morimoto Y, Cho B, Sohn H, Sandhu A. Porous-silicon photonic-crystal platform for the rapid detection of nano-sized superparamagnetic beads for biosensing applications. Nanosci Nanotechnol Lett 2011;3:612–616.
6. Bogaerts W, De Heyn P, Van Vaerenbergh T, De Vos K, Kumar Selvaraja S, Claes T, Dumon P, Bienstman P, Van Thourhout D, Baets R. Silicon microring resonators. Laser Photonics Rev 2012; 6:47–73.
7. Sun W, Puzas JE, Sheu T-J, Fauchet PM. Porous silicon as a cell interface for bone tissue engineering. Phys Status Solidi A 2007; 204:1429–1433.
8. Coffer JL, Whitehead MA, Nagesha DK, Mukherjee P, Akkaraju G, Totolici M, Saffie RS, Canham LT. Porous silicon-based scaffolds for tissue engineering and other biomedical applications. Phys Status Solidi A 2005;202:1451–1455.
9. Wu EC, Park J-H, Park J, Segal E, Cunin Fdr, Sailor MJ. Oxidation-triggered release of fluorescent molecules or drugs from mesoporous Si microparticles. ACS Nano 2008;2:2401–2409.
10. Salonen J, Laitinen L, Kaukonen AM, Tuura J, Björkqvist M, Heikkilä T, Vähä-Heikkilä K, Hirvonen J, Lehto VP. Mesoporous silicon microparticles for oral drug delivery: Loading and release of five model drugs. J Controlled Release 2005;108:362–374.
11. Parodi A, Quattrocchi N, van de Ven AL, Chiappini C, Evangelopoulos M, Martinez JO, Brown BS, Khaled SZ, Yazdi IK, Enzo MV, Isenhart L, Ferrari M, Tasciotti E. Synthetic nanoparticles functionalized with biomimetic leukocyte membranes possess cell-like functions. Nat Nanotechnol 2013;8:61–68.
12. Prestidge CA, Barnes TJ, Lau CH, Barnett C, Loni A, Canham L. Mesoporous silicon: A platform for the delivery of therapeutics. Expert Opin Drug Deliv 2007;4:101–110.
13. Low SP, Voelcker NH, Canham LT, Williams KA. The biocompatibility of porous silicon in tissues of the eye. Biomaterials 2009;30: 2873–2880.
14. Jurkic LM, Cepanec I, Pavelic SK, Pavelic K. Biological and therapeutic effects of ortho-silicic acid and some ortho-silicic acid-releasing compounds: New perspectives for therapy. Nutr Metab (Lond) 2013;10:2.
15. Jugdaohsingh R, Reffitt DM, Oldham C, Day JP, Fifield LK, Thompson RP, Powell JJ. Oligomeric but not monomeric silica prevents aluminum absorption in humans. Am J Clin Nutr 2000; 71:944–949.
16. Kawahara M, Kato-Negishi M. Link between aluminum and the pathogenesis of Alzheimer's disease: The integration of the aluminum and amyloid cascade hypotheses. Int J Alzheimers Dis 2011;2011:276393.

17. Reffitt DM, Ogston N, Jugdaohsingh R, Cheung HF, Evans BA, Thompson RP, Powell JJ, Hampson GN. Orthosilicic acid stimulates collagen type 1 synthesis and osteoblastic differentiation in human osteoblast-like cells in vitro. Bone 2003;32:127–135.
18. Chiappini C, Tasciotti E, Fakhoury JR, Fine D, Pullan L, Wang YC, Fu L, Liu X, Ferrari M. Tailored porous silicon microparticles: Fabrication and properties. Chemphyschem 2010;11:1029–1035.
19. Tasciotti E, Liu X, Bhavane R, Plant K, Leonard AD, Price BK, Cheng MM-C, Decuzzi P, Tour JM, Robertson F, Ferrari M. Mesoporous silicon particles as a multistage delivery system for imaging and therapeutic applications. Nat Nano 2008;3:151–157.
20. Ananta JS, Godin B, Sethi R, Moriggi L, Liu X, Serda RE, Krishnamurthy R, Muthupillai R, Bolskar RD, Helm L, Ferrari M, Wilson LJ, Decuzzi P. Geometrical confinement of gadolinium-based contrast agents in nanoporous particles enhances T1 contrast. Nat Nanotechnol 2010;5:815–821.
21. Tanaka T, Mangala LS, Vivas-Mejia PE, Nieves-Alicea R, Mann AP, Mora E, Han HD, Shahzad MM, Liu X, Bhavane R, Gu J, Fakhoury JR, Chiappini C, Lu C, Matsuo K, Godin B, Stone RL, Nick AM, Lopez-Berestein G, Sood AK, Ferrari M. Sustained small interfering RNA delivery by mesoporous silicon particles. Cancer Res 2010;70:3687–3696.
22. Godin B, Gu J, Serda RE, Bhavane R, Tasciotti E, Chiappini C, Liu X, Tanaka T, Decuzzi P, Ferrari M. Tailoring the degradation kinetics of mesoporous silicon structures through PEGylation. J Biomed Mater Res A 2010;94:1236–1243.
23. Bimbo LM, Makila E, Laaksonen T, Lehto VP, Salonen J, Hirvonen J, Santos HA. Drug permeation across intestinal epithelial cells using porous silicon nanoparticles. Biomaterials 2011;32:2625–2633.
24. Martinez JO, Chiappini C, Ziemys A, Faust AM, Kojic M, Liu X, Ferrari M, Tasciotti E. Engineering multi-stage nanovectors for controlled degradation and tunable release kinetics. Biomaterials 2013;34:8469–8477.
25. Martinez JO, Boada C, Yazdi IK, Evangelopoulos M, Brown BS, Liu X, Ferrari M, Tasciotti E. Short and long term, in vitro and in vivo correlations of cellular and tissue responses to mesoporous silicon nanovectors. Small 2013;9:1722–1733.
26. Genzel Y, Konig S, Reichl U. Amino acid analysis in mammalian cell culture media containing serum and high glucose concentrations by anion exchange chromatography and integrated pulsed amperometric detection. Anal Biochem 2004;335:119–125.
27. Sailor MJ. Fundamentals of Porous Silicon Preparation. Porous Silicon in Practice. Germany: Wiley-VCH Verlag GmbH & Co. KGaA; 2011. p 1–42.
28. Carlisle EM. Silicon: An essential element for the chick. Science 1972;178:619–621.
29. Martinez JO, Parodi A, Liu X, Kolonin MG, Ferrari M, Tasciotti E. Evaluation of cell function upon nanovector internalization. Small 2013;9:1696–1702.